Gynecologic Oncology 152 (2019) 396–407

Contents lists available at ScienceDirect

Gynecologic Oncology

journal homepage: www.elsevier.com/locate/ygyno

A clinical, biologic and mechanistic analysis of the role of ZNF692 in cervical cancer

Biqing Zhu [a,e,1], Yinpeng Pan [b,e,h,1], Xiufen Zheng [e,f,1], Quanli Zhang [e], Yaqin Wu [a,e], Jing Luo [g], Qian Li [a], Emei Lu [a], Lin Xu [b,e,*], Guangfu Jin [c,d,**], Binhui Ren [b,e,***]

[a] Department of Radiation Oncology, Jiangsu Cancer Hospital, Jiangsu Institute of Cancer Research, the Affiliated Cancer Hospital of Nanjing Medical University, China
[b] Department of Thoracic Surgery, Jiangsu Cancer Hospital, Jiangsu Institute of Cancer Research, the Affiliated Cancer Hospital of Nanjing Medical University, China
[c] Department of Epidemiology, School of Public Health, Nanjing Medical University, China
[d] Jiangsu Key Laboratory of Cancer Biomarkers, Prevention and Treatment, Collaborative Innovation Center for Cancer Medicine, Nanjing Medical University, China
[e] Jiangsu Key Laboratory of Molecular and Translational Cancer Research, China
[f] Department of Clinical Pharmacy, China Pharmaceutical University, China
[g] Department of Cardiothoracic Surgery, Jinling Hospital, Medical School of Nanjing University, China
[h] Department of Thoracic Surgery, the First People's Hospital of Lianyungang City Affiliated with Lianyungang Clinical College of Nanjing Medical University, Nanjing, Jiangsu, China

HIGHLIGHTS

- ZNF692 promotes proliferation, migration and invasion of cervical cancer.
- ZNF692 enhanced the G1/S transition via regulating the $p27^{kip1}/p^{Thr160}$-CDK2 signal pathway.
- ZNF692 directly binds to the promoter region of $p27^{kip1}$, which may provide therapeutic target.

ARTICLE INFO

Article history:
Received 2 September 2018
Received in revised form 12 November 2018
Accepted 13 November 2018
Available online 19 November 2018

Keywords:
Cervical cancer
Cell cycle
G1/S
$p27^{kip1}$
ZNF692

ABSTRACT

Objective. Cervical cancer (CC) is the most common malignancy in women. The zinc finger protein 692 (ZNF692) has been identified as a transcription factor and its aberrant expression participates in tumorigenesis of various cancers. However, its biological function and molecular mechanisms in cervical cancer remain unclear.

Methods. Microarrays were analysed by immunohistochemistry (IHC) to investigate the expression of ZNF692 in cervical cancer and its relationship with clinicopathologic characteristics. siRNAs and expression plasmids were used to reveal the biological function of ZNF692 in CC and subcutaneous xenograft model to examine the role of ZNF692 in vivo. Chromatin Immunoprecipitation and luciferase reporter assay were performed to ascertain whether ZNF692 binds to the promoter region of $p27^{kip1}$.

Results. By analyzing The Cancer Genome Atlas (TCGA) dataset, we confirmed ZNF692 as a potential oncogene in CC. ZNF692 expression was up-regulated in CC tissues compared with that in adjacent normal tissues, and its overexpression was correlated with poor clinicopathologic characteristics. Moreover, ZNF692 promoted the proliferation, migration and invasion of CC cells both in vitro and in vivo. Regarding molecular mechanisms, up-regulation of ZNF692 was found to enhance the G1/S transition via regulating the $p27^{kip1}/P^{Thr160}$-CDK2 signal pathway in CC cells.

Conclusion. ZNF692 promotes CC cells proliferation and invasion through suppressing $p27^{kip1}$ transcription by directly binding its promoter region, which suggests that ZNF692 may serve as an underlying therapeutic target and prognostic marker in CC.

* Correspondence to: L. Xu, Department of Thoracic Surgery, Jiangsu Cancer Hospital, Jiangsu Institute of Cancer Research, The Affiliated Cancer Hospital of Nanjing Medical University, Jiangsu Key Laboratory of Molecular and Translational Cancer Research, 42 Baiziting Road, Nanjing 210009, China.
** Correspondence to: G. Jin, Department of Epidemiology, School of Public Health, Jiangsu Key Laboratory of Cancer Biomarkers, Prevention and Treatment, Collaborative Innovation Center for Cancer Medicine, Nanjing Medical University, Nanjing 211166, China.
*** Correspondence to: Binhui Ren, Department of Thoracic Surgery, Jiangsu Cancer Hospital, Jiangsu Institute of Cancer Research, the Affiliated Cancer Hospital of Nanjing Medical University, 42 Baiziting Road, Nanjing 210009, China.
E-mail addresses: xulin83@njmu.edu.cn (L. Xu), guangfujin@njmu.edu.cn (G. Jin), renbinhui@jszlyy.com.cn (B. Ren).
[1] Equal contributors.

https://doi.org/10.1016/j.ygyno.2018.11.022
0090-8258/

1. Introduction

Cervical cancer (CC) is one of the most common gynaecological malignancies among women worldwide [1], and it remains a leading cause of cancer-related death for women in developing countries [2]. Despite improvements in therapeutic strategies over the last two decades, the prognosis remains poor [3,4]. The progression of CC is associated with various molecular alterations, but these molecular mechanisms have not been completely elucidated. Therefore, clarifying the molecular mechanisms of CC and identifying novel diagnostic markers and potential therapeutic targets are necessary to improve the survival of these patients.

Classical zinc finger-containing proteins (ZNFs), one of the three types of transcription factors, are encoded by 2% of human genes and constitute the largest family of sequence-specific DNA binding proteins [5,6]. Recent research has indicated that aberrant expression of ZNF proteins leads to tumorigenesis in various malignancies [7–9]. Although many studies have investigated the roles of ZNF proteins in various tumours, the biological function of ZNF692 has rarely been reported. ZNF692 is located on chromosome 1q44 and can bind to the promoter region of key genes to regulate the tumour progression as a transcription factor [10]. A previous study indicated that ZNF692 was related to the recurrence of Wilms tumours [11]. Additionally, ZNF692 has different RNA splicing patterns in various types of hepatocellular carcinoma [12]. Furthermore, our previous research suggests that ZNF692 is upregulated in lung adenocarcinoma (LUAD) and promotes the aggressiveness of LUAD [13]. Nevertheless, none of these studies have focused on the expression profile and molecular mechanisms of ZNF692 in CC.

To explore the role of ZNF692 in CC, we investigated the expression profiles of ZNF692 in the TCGA dataset, CC tissue microarrays and CC cell lines. Our results suggest that ZNF692 plays an important role in promoting aggressiveness, including proliferation, migration and invasion capacities in CC, by regulating the $p27^{kip1}$/P^{Thr160}-CDK2 signal pathway to induce the G1/S transition. Thus, ZNF692 might serve as a useful prognostic biomarker and a potential target in cervical carcinoma.

2. Material and methods

2.1. Bioinformatics analysis

A TCGA dataset termed TCGA_CESC_exp_HiS-eqV2-2015-02-24 was downloaded from the UCSC cancer browser (https://genome-cancer.ucsc.edu/) [14]. A total of 292 patients with complete clinical and follow-up information were extracted for further statistical analysis. Totally 387 genes which had the highest co-expression correlation with ZNF692 ($r > 0.4$ or $r < -0.4$) in the TCGA cervical cancer dataset were submitted to DAVID Bioinformatics Resources 6.7 (http://david.abcc.ncifcrf.gov/) [15,16] for Kyoto Encyclopaedia of Genes and Genomes (KEGG) and Gene Ontology (GO) pathway enrichment analysis. And GEPIA (Gene Expression Profiling Interactive Analysis) (http://gepia.cancer-pku.cn/index.html) was used to analyse the expression of ZNF692 with Disease Free Survival (DFS) of CC patients.

2.2. CC tissue microarrays analysis by immunohistochemistry (IHC)

For IHC assays based on tissue microarrays (TMAs), sixty-two pairs of paraffin-embedded human cervical cancer sections were analysed for ZNF692 expression by IHC according to a previous protocol [17]. Paired CC tissue microarrays were obtained from Shanghai Outdo Biotech Co., Ltd. (Cat. No. OD-CT-RpUtr 03-004 and OD-CT-RpUtr03-006). And the detailed information of CC cases was shown in Table S1. All tissues were examined by two experienced pathologists who confirmed the TNM stage of each patient. The UICC/AJCC TNM staging method (7th edition) was used for clinical staging and the lymph node metastasis was confirmed by dissecting lymph nodes during surgery. The sections were incubated with an anti-ZNF692 primary antibody (1:100 dilution; Abcam, ab204595). Tissue microarrays were assessed by two separate investigators blinded to the clinical parameters and then were subjected to statistical analysis. The IHC scores were calculated according to intensity and percentage of positive cells. The staining intensity was evaluated as the basis of 4 grades: 0 (negative staining), 1 (weak staining), 2 (moderate staining), or 3 (strong staining). The product (percentage of positive cells and respective intensity scores) was used as the final staining scores (a minimum value of 0 and a maximum value of 300).

2.3. Cell lines and cell culture

HeLa, C33a and Caski cervical cancer cell lines were purchased from American Type Culture Collection (ATCC, USA), and Siha and Hacat cell lines (normal human skin keratinocytes) were obtained from KeyGEN BioTECH (KeyGEN,Nanjing, China). HeLa, Siha, C33a and Hacat cells were incubated in DMEM medium (KeyGEN, Nanjing, China), while Caski cells were cultured in RPMI1640 (KeyGEN, Nanjing, China) medium containing 10% foetal bovine serum (GIBCO-BRL, Invitrogen, Carlsbad, CA, USA) in a humidified CO_2 incubator (Thermo Scientific, Waltham, MA, USA) at 37 °C in a 5% CO_2 environment.

2.4. siRNA, shRNA and plasmid transfection

Transfection was performed following the small-interfering RNA (siRNA) sequence transfection protocol for Lipofectamine RNAi MAX (Invitrogen, USA). Nonsense RNAi (nsRNA) was used as a negative control for siRNA. Transfection efficiency was evaluated by quantitative real-time PCR (qRT-PCR) and western blotting. All siRNA sequences (Realgene, Shanghai) are presented in Table S2.

Flag-ZNF692 cDNA was cloned into a pcDNA3.1 vector (GENEray Biotechnology) to construct an overexpression plasmid and an empty plasmid was used as a negative control. The small hairpin RNA (shRNA) for ZNF692 was generated according to si2-RNA sequence which was more efficient in knocking down ZNF692 (GENEray Biotechnology). Transfections of shRNA and plasmids were performed according to the Lipofectamine 3000 Reagent (Invitrogen, Carlsbad, CA, USA) protocol. The cells were transfected with pcDNA3.1-ZNF692 or vector, sh-ZNF692 or sh-NC, respectively [18].

2.5. RNA preparation, reverse transcription, and qRT-PCR

Total RNA was extracted from cells using TRIzol reagent (Invitrogen, Carlsbad, CA, USA) according to the manufacturer's protocol. Approximately 1500 ng of total RNA was reverse-transcripted in a final volume of 20 μL using a Reverse Transcription Kit (Takara, cat: RR036A) to produce cDNA. qRT-PCR was conducted using SYBR Select Master Mix (Applied Biosystems. Cat: 4472908). The relative expression of each product was normalized to the expression of β-actin. Primers used to amplify ZNF692, $p15^{ink4b}$, $p16^{ink4a}$, $p21^{cip1}$, $p27^{kip1}$, CCNB1, CCND1, CCNE1, CDK2, CDK4 and CDK6 are shown in Table S3 (Realgene, Shanghai, China). qRT-PCR was done on a QuantStudioTM 6 Flex Real-Time PCR system using the following programme: 1 cycle at 95 °C for 10 min followed by 40 cycles at 92 °C for 15 s and 60 °C for 1 min.

2.6. Protein preparation and western blotting

Transfected cells were harvested and protein was extracted using RIPA Lysis Buffer (Kaiji, Nanjing, China) according to the instructions provided by the manufacturer. Protein samples (40 μg) were loaded into 10% sodium dodecyl sulfate polyacrylamide electrophoresis (SDS-PAGE) gels and transferred onto a PVDF membrane after electrophoresis. The membrane was blocked with non-fat milk for 2 h, and incubated overnight with antibodies against ZNF692 (Abcam, 1:200), $p21^{cip1}$, $p27^{kip1}$, CCNE1, CDK2, P^{Thr160}-CDK2, CCND1, CCNB1 or β-actin (Cell Signalling, 1:1000). After washing with TBST for 3 times, the membrane

was incubated with goat anti-rabbit or anti-mouse HRP-conjugated secondary antibody (Abcam, 1: 10,000) for 2 h at room temperature in the dark. The bands were visualized by ECL detection (Thermo Scientific). All experiments were repeated triplicate.

2.7. xCELLigence System assay

Cell proliferative ability was measured using a real time xCELLigence system (RTCA) according to the instructions provided by the manufacturer [19]. Briefly, the cells were collected and counted in a blood-counting chamber after transfection with siRNA, si-NC, oe-ZNF692 or vector for 24 h. The cells were then resuspended in medium with FBS and seeded in E-plates at a density of 8,000 per well. The E-plates were placed into the RTCA device in the incubator. The proliferation was automatically detected by the xCELLigence system and outputted as a cell index value. The cell index was monitored in real-time at least 60 h.

2.8. Colony formation assay

The transfected cells were placed in 6-well plates at 400 cells per well for colony formation assays. The media were changed every 5 days. After 10–14 days, the cells were fixed using 4% paraformaldehyde and stained with 0.1% crystal violet solution. Visible clones which contained at least 50 cells were manually counted. Each experiment was repeated 3 times.

2.9. Ethynyl-2-deoxyuridine (EdU) incorporation assay

Cell proliferation was also determined using a ethynyl-2-deoxyuridine incorporation assay with the keyFluor488 Click-IT EDU Kit (KeyGENBioTECH, Nanjing, China) according to the manufacturer's protocol [20]. Briefly, the transfected cells were placed in 96-well plates (8000 cells/well) overnight in a CO_2 incubator. Then, cells were incubated with 100 μL/well of 10 μM EdU for 2 h at 37 °C and fixed with 50 μL 4% paraformaldehyde-containing PBS for 30 min at room temperature. Subsequently, the cells were cultured for 5 min with 50 μL of 2 mg/mL glycine and then washed with 100 μL 3% BSA in PBS. After permeabilization with 0.5% Triton X-100 for 20 min, the cells were cultured with 1 × Click-iT reaction solution for 30 min at room temperature in dark conditions. After that, cells were incubated with 100 μL/well of 1 × Hoechst 33342 solutions for 30 min at room temperature in the dark after washing with 100 μL of PBS. The cells were then imaged using fluorescence microscopy and proliferation cells ratios were counted from 5 random fields in every well. Each experiment was repeated 3 times.

2.10. Migration and invasion assay

A total of 40,000 transfected cells were added to the upper chamber of Transwell assay inserts (8 μM PET, 24-well Millicell) or a Matrigel-coated membrane (BD Biosciences) containing 200 μL serum-free DMEM media. The lower chambers were filled with 800 μL DMEM media containing 10% FBS. After a 24-h (migration assay) or 48-h (invasion assay) incubation, the cells were fixed with 4% paraformaldehyde, stained with crystal violet, and imaged. Migration and invasion were assessed by counting cell nuclei from 5 random fields on every filter. Each Experiment was repeated three times.

2.11. Wound healing assay

The cells were placed on six-well plates and transfected with si-ZNF692, si-NC, pcDNA3.1-ZNF692 or vector as described above. After 24 h, an artificial scratch wound on a confluent monolayer of cells was generated using a 200 μL pipette tip. Serum-free medium was added for 48 h, and the cells were imaged. Each assay was repeated three times.

2.12. Flow cytometry assay

Cell cycle distribution was measured by flow cytometry. Cells were harvested after transfection with siRNA for 48 h and fixed in 1 mL 70% ethanol at −20 °C. Then, the cells were stained with propidium iodide (PI) following the manufacturer's instructions [21]. The cells were then analysed using a FACScan flow cytometer (Becton Dickinson, Franklin Lakes, NJ). The percentage of the cell cycle in G1, S, and G2/M phase were displayed in a bar graph. All the samples were performed in triplicate.

2.13. ChIP assay

The adherent HeLa and Siha cells were cross-linked in 4% paraformaldehyde for 10 min, and the reaction was terminated with 10 × glycine. After two washes with cold PBS, cells were scraped into new 1.5 mL centrifuge tube after adding 1.0 mL cold PBS (containing 5 μL protease inhibitor, cocktail) and centrifuged for 10 min at 800 ×*g* at 4 °C. Pelleted cells were resuspended in 500uL cell lysis buffer (containing 2.5 μL cocktail) and incubated on ice for 15 min, then the cells were centrifuged for 5 min at 800 ×*g*, 4 °C. Cell precipitates were resuspended in 500uL nucleus lysis buffer (containing 2.5 μL cocktail) successively. After that, the cells were sonicated (amplitude 30%) on ice for 10 min to break DNA into fragments. And the product was centrifuged for 10 min at 12,000*g* at 4 °C. Specific anti-Flag antibody (SIGMA, F1804) coupled to magnetic beads (Resin M2, Sigma, Shanghai, China) was used to immunoprecipitate the DNA-protein complex, and the IgG antibody was used as a negative control. The beads were then washed with 500uL low salt buffer, high salt buffer, LiCi buffer, and TE buffer successively, all for 5 min at 4 °C. The beads were added with elution buffer (containing proteinase K) and then heated at 62 °C for 2 h and 95 °C for 10 min. Next the beads were removed in magnetic frame and the supernatant was transferred into a new tube. In the last step, the supernatant was added with Bind reagent A and put in adsorption column. After washed with Wash reagent B, the DNA was eluted with elution buffer C from adsorption column and used for PCR reaction. PCR was performed with MasterMix with 7 primes as shown in Table S4.

2.14. Luciferase reporter assay

The promoter of $p27^{kip1}$ cDNA cDNA (700–1200 bp) was amplified by using PCR and cloned into luciferase reporter plasmids (pGL3-basic). The luciferase reporter plasmids were co-transfected with pcDNA3.1-ZNF692 or si-ZNF692 in HEK293T cells. After 48 h, cells were harvested and assessed for luciferase activity using the Dual Luciferase Reporter Assay System (Promega, Madison, WI, USA). Relative luciferase activity was corrected for Renilla luciferase activity of pGL3-basic, and normalized to the activity of the control (pcDNA3.1 or si-NC).

2.15. Animal study

The experimental protocols were evaluated and approved by the Nanjing Medical Animal Care Committee. Eight female nude mice (4–6 weeks old) were purchased from Nanjing Medical University School of Medicine's accredited animal facility. HeLa cells were transfected with sh-ZNF692 or sh-NC as previously described, and 5.0×10^6 logarithmic growth cells were implanted subcutaneously in the armpit of the mice. Tumour volume (length × width^2 × 0.5) was measured weekly using callipers. Four weeks after injection, the animals were sacrificed, and the tumours were measured. Meanwhile, the tumour tissues were immunohistochemically stained with ZNF692 (Abcam, 1:200), Ki67 (Spring Bioscience, 1:100), and $p27^{kip1}$ (Cell Signalling, 1:200).

2.16. Statistical analysis

Data are shown as the means ± S.D., and Student's *t*-test, chi-square test, one-way ANOVA were used to analyse the data using SPSS statistics software (version 20.0, Chicago, III). $P < 0.05$ was considered statistically significant.

3. Results

3.1. ZNF692 was identified as a candidate oncogene in CC

Analysis of TCGA_CESC_exp_HiSeqV2-2015-02-24 dataset showed that average expression of ZNF692 (9.448 ± 0.03757, $n = 303$) in CC tissues was higher than that in adjacent normal tissues (8.615 ± 0.2145, n = 3) ($p = 0.0285$, Fig. 1A). And there was no statistical difference between the expression of ZNF692 in CIN III and normal cervical tissues (Fig. S1). ZNF692 expression in stage III-IV patients (9.586 ± 0.07997, $n = 65$) was up-regulated compared with stage I-II patients (9.402 ± 0.04356, $n = 227$) ($p = 0.0453$, Fig. 1B), and ZNF692 mRNA expression was elevated in patients of T2–T3 stage (9.553 ± 0.07276, $n = 98$) compared with those of T1 stage (9.357 ± 0.05524, $n = 138$) ($p = 0.0299$, Fig. 1C). GEPIA analysis indicated that ZNF692 expression had negative correlation with the PFS of cervical cancer patients ($p = 0.03$, Fig. 1D). The expression profile of ZNF692 protein was further determined by IHC analysis in CC tissue microarrays. Representative IHC staining images of ZNF692 in TMAs are shown in Fig. 1E. ZNF692 staining scores were elevated in tumour tissues (214.6 ± 5.706) as opposed to those in adjacent normal tissues (125.2 ± 4.270) ($n = 62$, $p < 0.0001$, Fig. 1F). Also, hyper-expression of ZNF692 was positively correlated with advanced TNM stages (III–IV VS I–II, 228.6 ± 7.069 VS 200.5 ± 8.321, $p = 0.0125$, Fig. 1G) and lymph node metastasis ((N1–N3 VS N0, 228.6 ± 7.069 VS 200.5 ± 8.321, p = 0.0125, Fig. 1H). Based on the expression value of ZNF692 in CC tissues, we divided the patients into two groups: ZNF692 high expression group ($n = 31$) and ZNF692 low expression group (n = 31). And results showed that patients with higher expression of ZNF692 tend to have more advanced stages in T stage ($p = 0.0387$), N stage ($p = 0.0223$) and TNM stage (p = 0.0223) (Table S5).

3.2. Knockdown of ZNF692 suppressed the aggressiveness of CC in vitro

The expression of ZNF692, as measured by qRT-PCR and western blot, was up-regulated in CC cell lines compared with that in normal human skin keratinocytes (Hacat cells) (Fig. 2A-B). HeLa and Siha cell lines were chosen to investigate the biological function of silencing ZNF692. Then, two different effective siRNAs were constructed to knockdown ZNF692, while transfection efficiency was determined by qRT-PCR and western blotting (Fig. 2C-F). The results of the colony formation assay revealed that a significant decrease in cell growth of HeLa (si-NC VS si1, 188.70 ± 15.30 VS 70.67 ± 6.64, $p = 0.0021$; si-NC VS si2, 188.70 ± 15.30 VS 31.67 ± 6.17, $p = 0.0007$) and Siha cells (si-NC VS si1, 138.70 ± 11.62 VS 60.00 ± 9.17, $p = 0.0060$; si-NC VS si2, 138.70 ± 11.62 VS 31.67 ± 3.76, $p = 0.0009$) in si-ZNF692 group compared to si-NC group (Fig. 2G). The xCELLigence system showed that proliferative ability of HeLa and Siha cells was inhibited in si-ZNF692 group (Fig. 2H) and the EdU incorporation assay indicated that the proliferation cells ratio declined in si-ZNF692 HeLa cells (si-NC VS si-ZNF692, 40.12 ± 2.62 VS 25.28 ± 1.59, $p = 0.0013$) and Siha cells (si-NC VS si-ZNF692, 36.92 ± 2.16 VS 24.56 ± 1.47, $p = 0.0015$) compared to si-NC group (Fig. 2I). The Transwell assay (HeLa, si-NC VS si-ZNF692, 160.6 ± 6.01 VS 73.80 ± 6.02, $p < 0.0001$; Siha, si-NC VS si-ZNF692, 120.8 ± 8.108 VS 50.40 ± 7.194, p = 0.002) and Matrigel invasion assay (HeLa, si-NC VS si-ZNF692, 142.6 ± 7.28 VS 55.40 ± 7.59, p < 0.0001; Siha, si-NC VS si-ZNF692, 118.25 ± 9.48 VS 33.40 ± 8.19, $p = 0.0002$) (Fig. 2J), and wound healing assay (Fig. 2K) found that migration and invasion abilities of HeLa and Siha cells were suppressed by knockdown of ZNF692. Meanwhile, si-ZNF692 treatment induced G1 phase arrest (HeLa, si-NC VS si-ZNF692, 44.62 ± 1.13 VS 62.03 ± 2.86, $p = 0.0048$; Siha, si-NC VS si-ZNF692, 47.75 ± 1.52 VS 60.78 ± 1.31, $p = 0.0029$) (Fig. 2L).

3.3. Overexpression of ZNF692 promoted the malignant phenotype in HeLa cells

To further verify the function of ZNF692, a pcDNA3.1-ZNF692 plasmid was transfected into HeLa cells. Transfection efficiency was measured by qRT-PCR (Fig. 3 A) and western blotting (Fig. 3 B). Overexpression of ZNF692 enhanced HeLa cell proliferation, as analysed by the xCELLigence system (Fig. 3C). EdU incorporation assay showed that the proliferation cells ratio increased in oe-ZNF692 HeLa cells compared to oe-NC group (oe-NC VS oe-ZNF692, 37.42 ± 1.73 VS 44.66 ± 1.23, $p = 0.0092$) (Fig. 3D) and colony formation assay also indicated the similar results (oe-NC VS oe-ZNF692, 207.0 ± 8.74 VS 307.7 ± 6.50, $p = 0.0008$) (Fig. 3E). We also found that ZNF692-overexpressing CC cells displayed increasing migration ability in wound healing assay (Fig. 3F), Transwell assay (oe-NC VS oe-ZNF692, 147.8 ± 5.68 VS 224.2 ± 8.59, $p < 0.0001$) and Matrigel invasion assay (oe-NC VS oe-ZNF692, 126.8 ± 7.70 VS 200.0 ± 9.73, $p = 0.0004$) (Fig. 3G).

3.4. ZNF692 promoted cell proliferation and invasion through suppressing $p27^{kip1}$ expression by directly binding its promoter region

GO analysis was used to elucidate how ZNF692 exerts its carcinogenic effect. As shown in Fig. 4A, most of the genes were enriched in regulation of transcription and many genes were enriched related to cell cycle regulation. Our present results showed that si-ZNF692 impaired CC cell proliferation and generated G1 phase arrest, which is consistent with the GO analysis results. Therefore, we evaluated expression of G1 phase-related cell cycle regulation genes, and the finding suggested that $p27^{kip1}$ was increased or decreased at the mRNA level after knockdown or ectopic expression of ZNF692 in CC cell lines, respectively (Fig. 4B-D). When ZNF692 was knocked down, $p27^{kip1}$ was obviously increased and P^{Thr160}-CDK2 expression was moderately decreased at the protein level; however, CDK2 and CCNE1 was not obviously affected at the protein level (Fig. 4E). Meanwhile, overexpression of ZNF692 showed the opposite results at the protein level (Fig. 4F). Moreover, the expression of $p15^{ink4b}$, $p16^{ink4a}$, $p21^{cip1}$, CCNB1, CCND1, CDK4, and CDK6 was not influenced either at the mRNA or the protein level (Fig. 4B-F).

ZNF proteins function as transcription factor by binding the specific nucleotide sequences of DNA [22]. To further verify whether ZNF692 binds to the promoter region of $p27^{kip1}$ to suppress its transcription, we performed ChIP assay. According to the sequence of promoter region, 7 primers are designed for different sections. After immunoprecipitation by Flag-ZNF692, the 7 primers were used for PCR. Results showed that only primer 5 (815–1022 bp) was enriched in the immunoprecipitation complex both in Siha and Hela cells. The PCR amplification product was then used for agarose gel electrophoresis, and compared with IgG group, Flag-ZNF692 enriched more DNA fragments amplified by primer 5 (Fig. 4G). In addition to this, ectopic ZNF692 or si-ZNF692 significantly reduced or increase luciferase activity when co-transfected PGL3-$p27^{kip1}$ promoter cDNA (700–1200 bp) (Fig. 4H). These results suggest that ZNF692 directly binds the promoter region of $p27^{kip1}$ to suppress its transcription.

3.5. Downregulation of $p27^{kip1}$ partially recovered the phenotypes of si-ZNF692 cells

Finally, a rescue experiment was designed to demonstrate that ZNF692 performed its carcinogenic activity in a $p27^{kip1}$-dependent manner. The knockdown efficiencies of two siRNA sequences directed

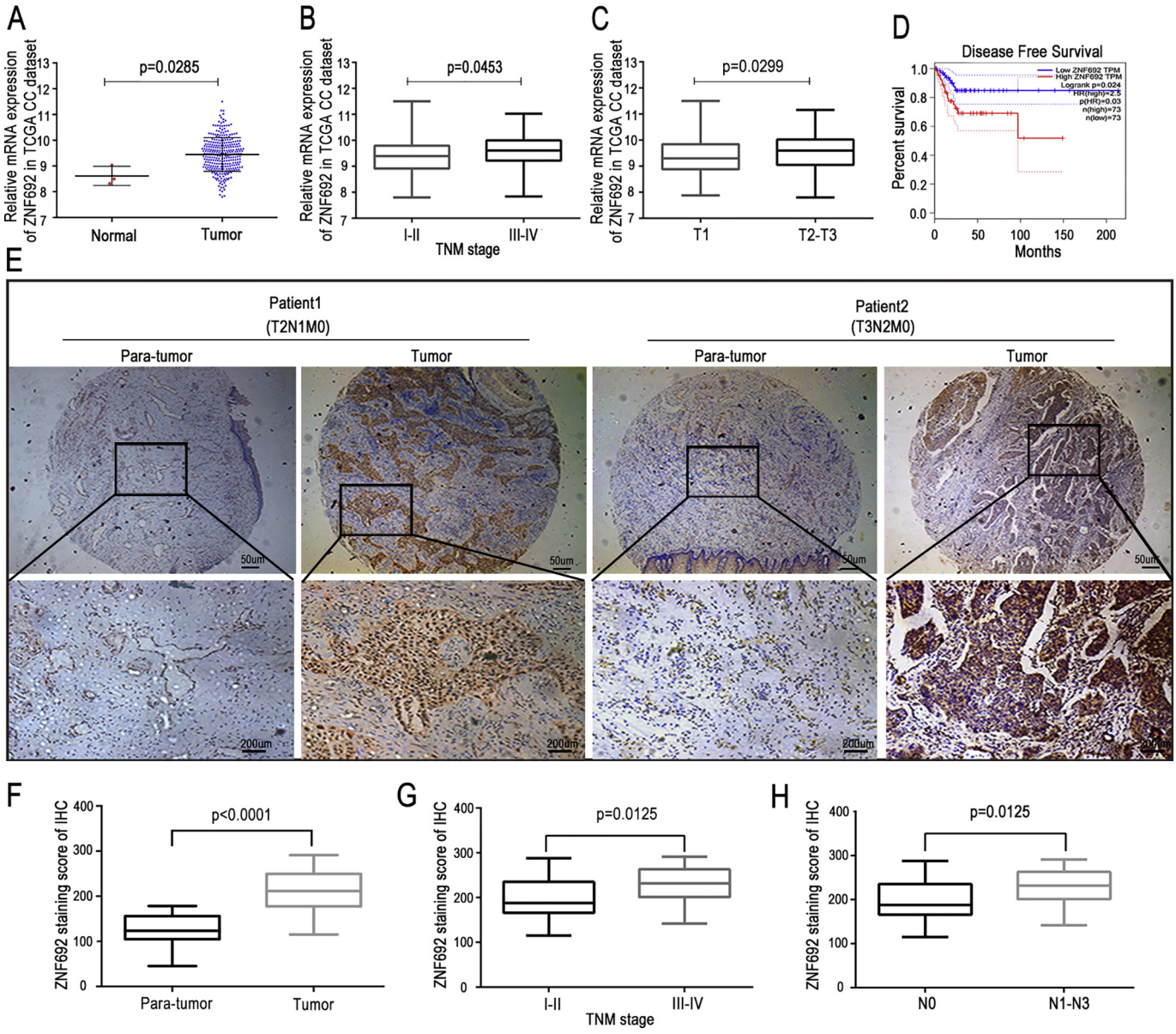

Fig. 1. ZNF692 was over-expressed in CC tissues and positively correlated with more aggressive clinical characteristics. (A) ZNF692 was up-regulated in CC tissues compared with adjacent normal tissues in TCGA dataset ($P = 0.0285$). (B) ZNF692 was up-regulated in patients of stage III-IV compared with those of stage I-II by analysis of the TCGA dataset ($p = 0.0453$). (C) Overexpression of ZNF692 was positively associated with T stage according to the TCGA database. ($p = 0.0299$). (D) GEPIA analysis showed that the expression of ZNF692 had a negative correlation with the Disease Free Survival (DFS) of cervical cancer patients ($p = 0.03$). (E) Representative IHC staining images of TMAs are shown. (F) The ZNF692 staining score was increased in CC tissues compared with para-tumour tissues ($p < 0.0001$). (G-H) The ZNF 692 staining score was positively correlated with an advanced TNM stage ($p = 0.0125$) and lymph node metastasis ($p = 0.0125$) in CC tissues. Error bars represent the mean ± SD values.

toward $p27^{kip1}$ were first determined by qRT-PCR (Fig. 5A), and the si1-RNA sequence was chosen for further study. Then, si-ZNF692 HeLa cells were simultaneously transfected with si-$p27^{kip1}$ and $p27^{kip1}$ expression was measured by qRT-PCR and western blotting (Fig. 5B and G). Cell proliferation, migration and invasion capacities were partially recovered by downregulation of $p27^{kip1}$ as measured by the proliferation assay (Fig. 5C), colony formation assay (si-ZNF692 VS recovered group, 71.0 ± 7.51 VS 186.3 ± 4.26, $p = 0.0002$, Fig. 5D), EdU incorporation assay (si-ZNF692 VS recovered group, 27.86 ± 0.83 VS 36.02 ± 1.22, $p = 0.0006$, Fig. 5E). Transwell assays (si-ZNF692 VS recovered group, 73.67 ± 8.09 VS 161.7 ± 12.81, $p = 0.0044$) and Matrigel invasion assay (si-ZNF692 VS recovered group, 62.67 ± 6.57 VS 113.3 ± 10.40, $p = 0.0146$) (Fig. 5F). Moreover, upon simultaneous knockdown of $p27^{kip1}$ and ZNF692 in HeLa cells, the expression of P^{Thr160}-CDK2 was partially elevated, compared with si-ZNF692 alone in HeLa cells (Fig. 5G).

3.6. Knockdown of ZNF692 inhibited tumour growth in vivo

To estimate the oncogenic abilities of ZNF692 in vivo, we constructed a xenograft tumour model using HeLa cells transfected with sh-NC or sh-ZNF692 (Fig. S2). The interference efficiencies were determined by qRT-PCR and western blot (Fig. 6A–B). All nude female mice generated xenograft tumours at the injection sites, and xenograft tumours were collected 4 weeks after injection (Fig. 6C). Tumours volumes (Final volume, sh-NC VS sh-ZNF692, 1078.0 ± 130.1 VS 592.4 ± 61.12, $p = 0.0149$) and weights (sh-NC VS sh-ZNF692, 0.41 ± 0.013 VS 0.20 ± 0.008, $p < 0.0001$) declined in the sh-ZNF692 group

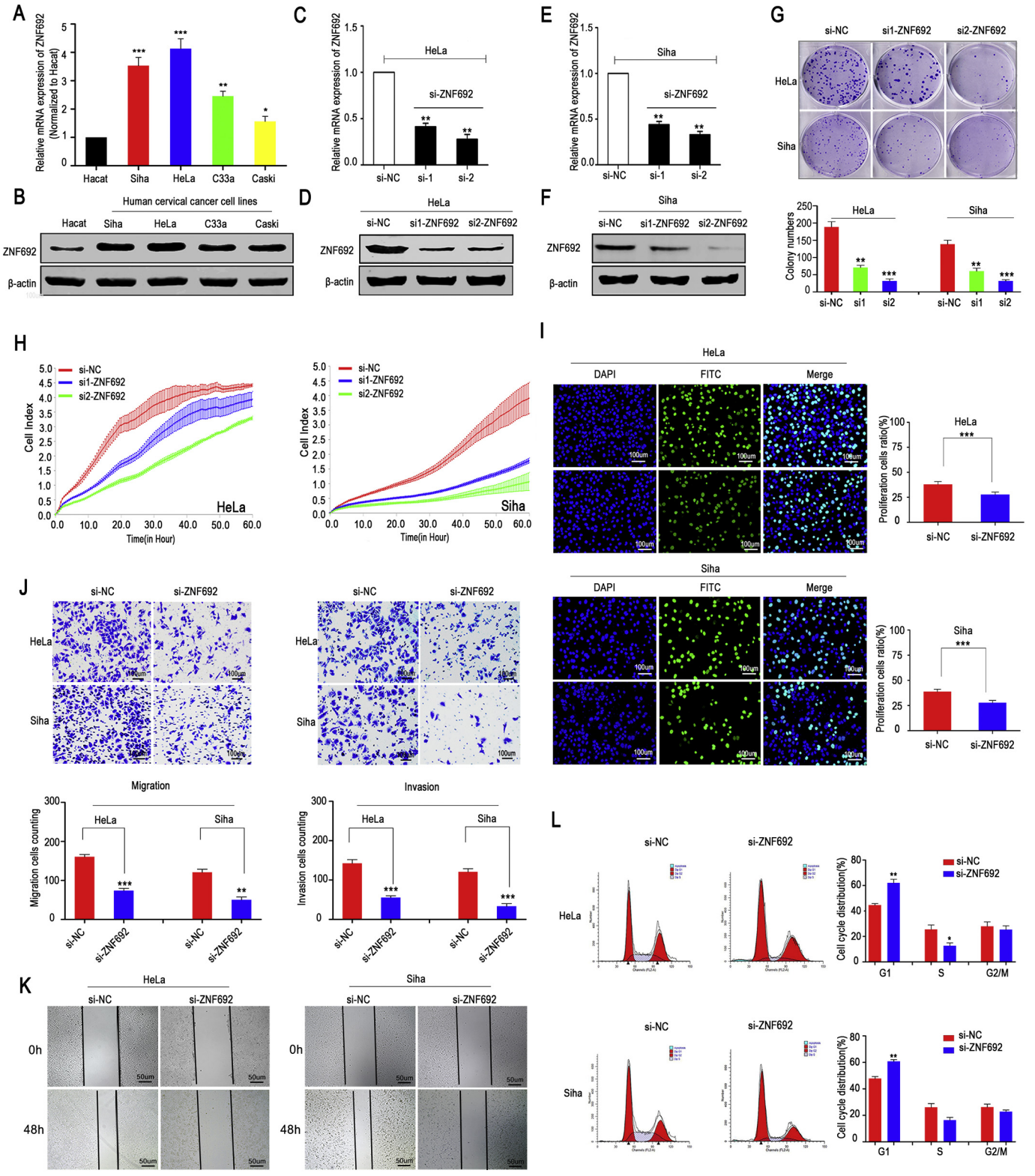

Fig. 2. Knockdown of ZNF692 inhibited the CC cell proliferation, migration, invasion and induced G1 cell cycle arrest in vitro. (A–B) ZNF692 mRNA and protein level are highly expressed in CC cell lines. (C–F) Two specific siRNA (si1 and si2) of ZNF692 were designed and the transfection efficiencies of siRNAs in HeLa and Siha cells were determined by qRT-PCR and western blotting. (G) Colony formation ability was inhibited by knockdown of ZNF692 in HeLa and Siha cells. (H) XCELLigence System assays also indicated that knockdown of ZNF692 inhibited proliferation of HeLa cells and Siha cells. (I) EdU incorporation assay revealed that knockdown of ZNF692 inhibited proliferation of HeLa cells and Siha cells. (J) Transwell assay and Matrigel assay and (K) wound healing assay revealed that migration and invasion abilities were suppressed by siRNA-mediated knockdown of ZNF692. (L) Knockdown of ZNF692 induced G1 cell cycle arrest measured by flow cytometry. Error bars represent the mean ± SD values of three independent experiments. $^{*}P < 0.05$, $^{**}P < 0.01$, $^{***}P < 0.001$.

compared with those in the sh-NC group (Fig. 6D-E). IHC analysis demonstrated that tumours derived from the sh-ZNF692 group showed weaker staining of ZNF692 and Ki-67 than those derived from the sh-NC group; meanwhile, $p27^{kip1}$ staining was increased in the sh-ZNF692 group (Fig. 6F). These findings inferred that sh-ZNF692 might suppress tumour growth and up-regulate $p27^{kip1}$ expression in vivo.

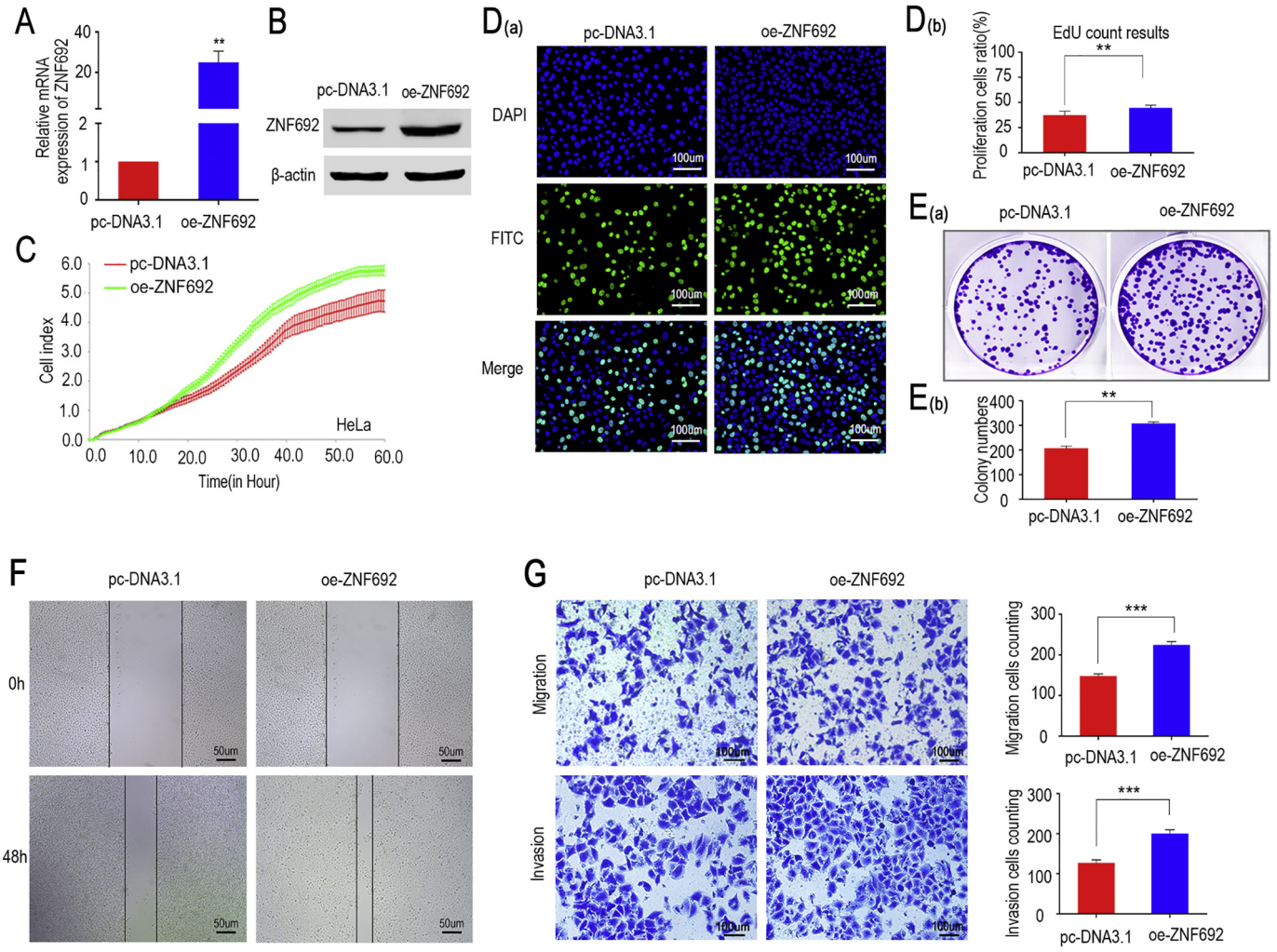

Fig. 3. Overexpression of ZNF692 promoted proliferation, migration and invasion of HeLa cells. (A–B) The pcDNA3.1-ZNF692 was synthesized and the transfection efficiencies of oe-ZNF692 were estimated by qRT-PCR and western blotting. (C–E) Ectopic expression of ZNF692 enhanced proliferation capacity of HeLa cells. (F–G) Overexpression of ZNF692 promoted migration and invasion of HeLa cells. Error bars represent the mean ± SD values of three independent experiments. *P < 0.05, **P < 0.01, ***P < 0. 001.

4. Discussion

This study indicated that ZNF692 played an important role in promoting aggressiveness in CC. Here, we firstly found that the expression of ZNF692 was upregulated in CC tissues compared with its expression in the adjacent normal tissues. Moreover, knockdown or ectopic expression of ZNF692 suppressed or promoted the proliferation and invasion abilities of CC cells, respectively. Furthermore, xenograft tumour models using HeLa cells showed that knockdown of ZNF692 inhibited tumour growth in vivo. Regarding its molecular mechanism, si-ZNF692 treatment of CC cells induced G1 phase arrest, upregulated $p27^{kip1}$ and downregulated P^{Thr160}-CDK2 expression while overexpression of ZNF692 suppressed $p27^{kip1}$ and promoted P^{Thr160}-CDK2 expression. Interestingly, Chromatin immunoprecipitation (ChIP) assay revealed that ZNF692 directly targeted $p27^{kip1}$ promoter region (815–1022 bp) and luciferase reporter assay indicated that ectopic or si-ZNF692 significantly reduced or increased $p27^{kip1}$ promoter (700-1200 bp) luciferase activity. Additionally, inhibition of $p27^{kip1}$ expression partially recovered the influence of si-ZNF692 on malignant phenotype in Hela cells. Taken together, our results provided evidence that ZNF692 promoted the progression of CC and might be a potential prognostic biomarker as well as the therapeutic target in CC.

The involvement of ZNF692 in cancer has been reported in many studies. For example, ZNF692 was up-regulated in the parous breast via transcription regulation and chromatin organization [23]. Our previous study demonstrated that down-regulation of ZNF692 could suppress tumour proliferation and invasion of lung adenocarcinoma cells and overexpression of ZNF692 is strongly associated with poorer survival in LUAD [13]. Similar to our previous findings, we found that ZNF692 was overexpressed in CC tissues compared with that in adjacent normal tissues and was negatively correlated with PFS in CC patients. Moreover, overexpression of ZNF692 was also positively correlated with advanced TNM stage and lymph node metastasis based on analysis of CC tissue microarrays.

By GO enrichment analyses, we found that the genes which had the highest correlation values with ZNF692 were enriched in regulation of transcription and the cell cycle. In the past decade, role of cell cycle dysregulation has been recognized in occurrence and progression of tumours [24–26]. There has been mounting evidence to indicate that metabolite profiling has a key role in the study of cancer cell proliferation [27,28] and a better understanding of the metabolic basis of cell cycle disorders is expected to uncover the mechanisms of accelerating tumorigenesis [29].

Our functional experiments were consistent with the GO analyses, in which knockdown of ZNF692 impaired CC cell proliferation, migration and invasion by inhibiting the G1/S phase transition. Therefore, we analysed several critical G1/S transition-related genes to illuminate a potential mechanism. Previous studies have reported that $p27^{kip1}$ arrests the cell cycle at the G1 phase by inhibiting the activation of the CCNE1-CDK2 complex [30–33]. The distribution and prognostic value

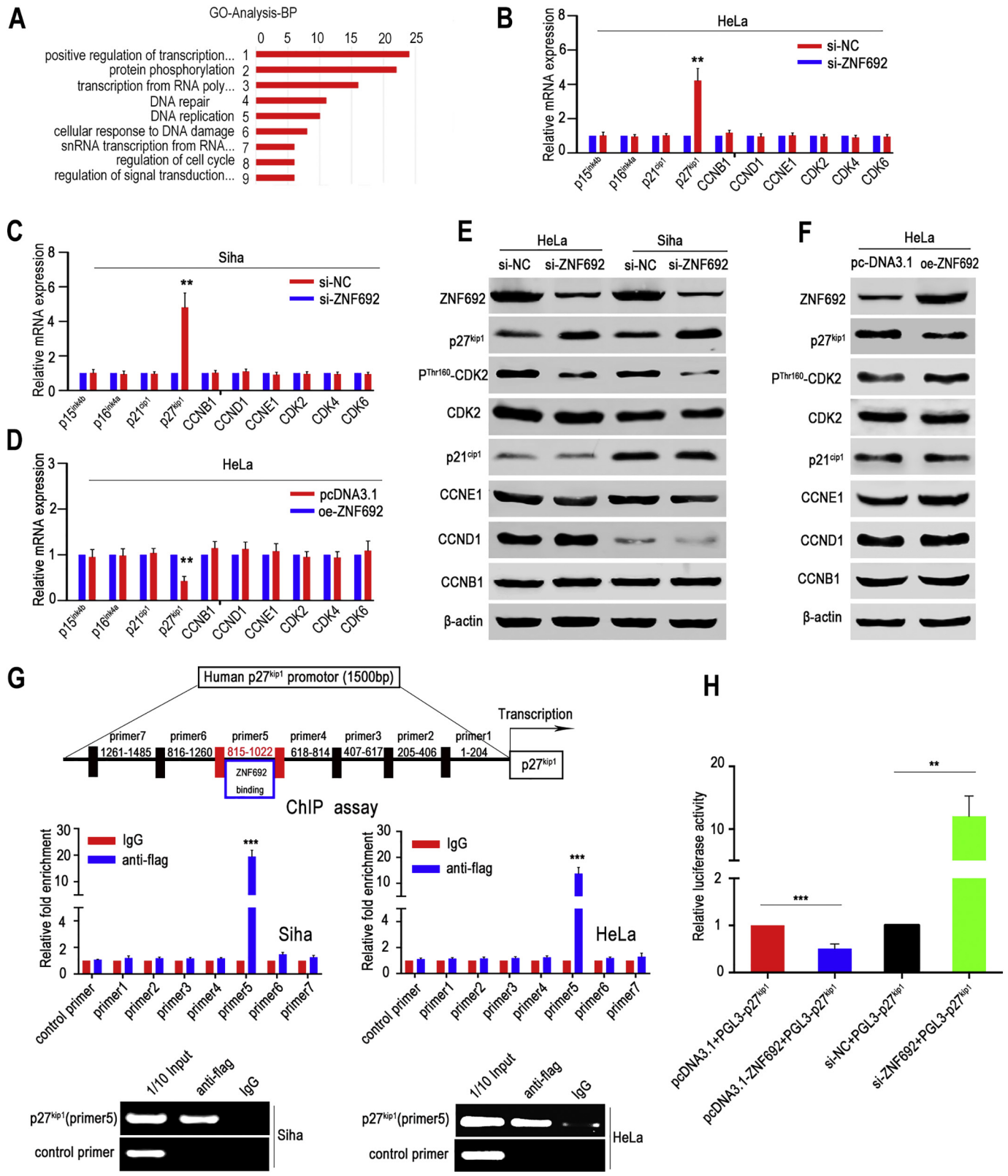

Fig. 4. ZNF692 suppressed the $p27^{kip1}$ expression by directly binding its promoter region. (A) Genes of high correlation with ZNF692 were enriched in regulation of transcription and cell cycle regulation by GO analysis. (B–D) The $p27^{kip1}$ mRNA levels were significantly increased or decreased after knockdown or ectopic expression of ZNF692 in CC cell lines, respectively. (E–F) The protein level of $p27^{kip1}$ was obviously upregulated or downregulated while the expression of P^{Thr160}-CDK2 was moderately decreased or increased in si- or oe-ZNF692 of CC cells. The expression of CDK2, CCNE1 was not obviously affected at the protein level after knockdown or ectopic expression of ZNF692 in CC cells. However, the $p21^{cip1}$, CCND1 and CCNB1 had no significant changes in si- or oe-ZNF692. (G) Each approximately 200 bp length was designed for 7 primers within 1500 bp of the $p27^{kip1}$ promoter region. Chromatin immunoprecipitation (ChIP) assays using normal IgG or anti-Flag-ZNF692 revealed that ZNF692 directly targeted $p27^{kip1}$ promoter region (815–1022 bp). (H) Ectopic ZNF692 or si-ZNF692 significantly reduced or increased $p27^{kip1}$ promoter (700–1200 bp) luciferase activity. Error bars represent the mean ± SD values of three independent experiments. *P < 0.05, **P < 0.01, ***P < 0. 001.

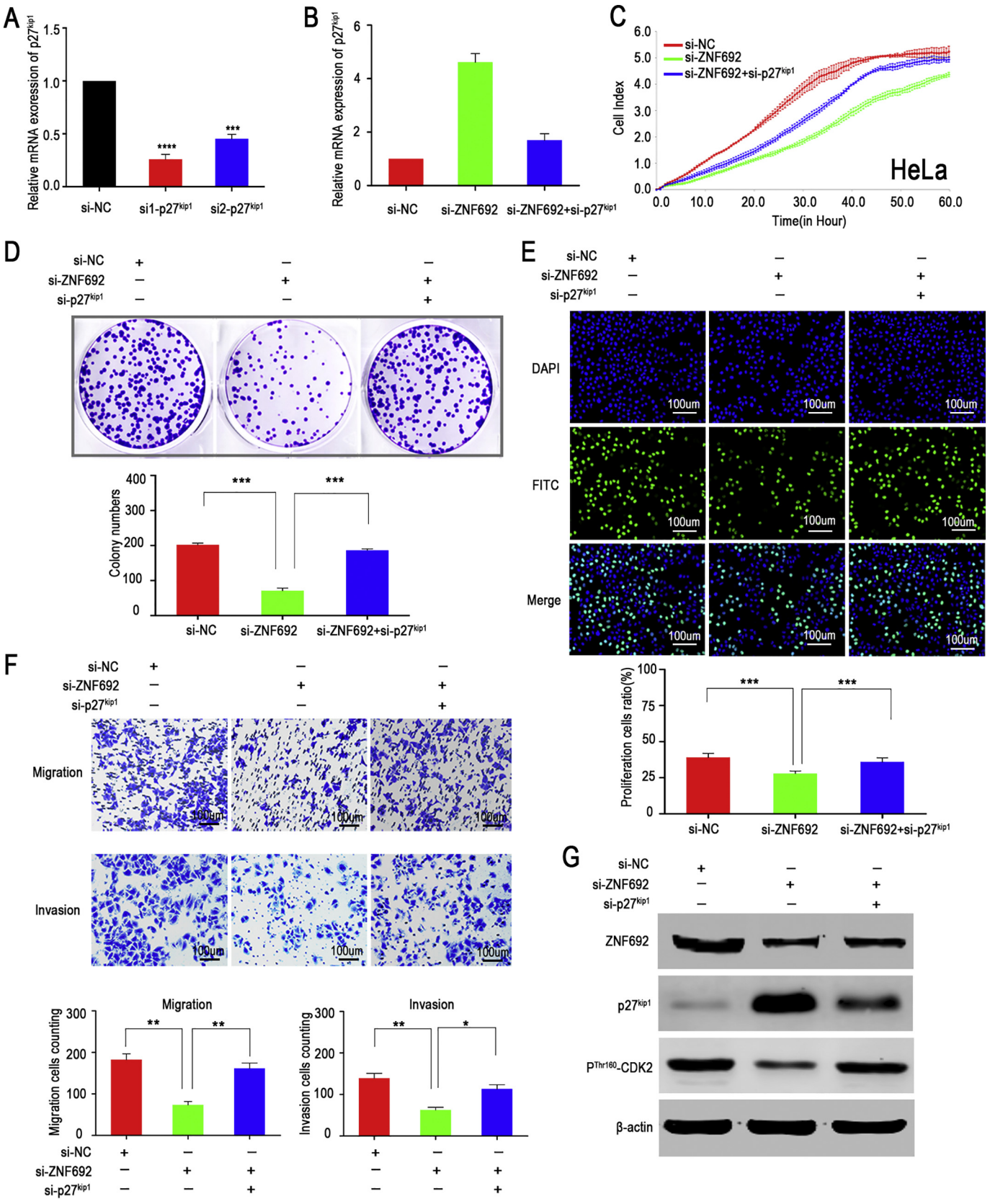

Fig. 5. Downregulation of p27kip1 partially reversed the phenotypes of si-ZNF692 cells. (A) The transfection efficiency of si-p27^{kip1} was determined by qRT-PCR. (B–D) The proliferative abilities were partially rescued after treatment with si-p27^{kip1} in si-ZNF692 HeLa cells. (E) Knockdown of p27^{kip1} partially reversed the inhibitory effect of si-ZNF692 on the migration and invasion of HeLa cells. (F) Western blotting showed that the expression of p27^{kip1} and P^{Thr160}-CDK2 were partially recovered after knockdown of p27^{kip1} in si-ZNF692 compared with si-ZNF692 alone in HeLa cells. Error bars represent the mean ± SD values of three independent experiments. *P < 0.05, **P < 0.01, ***P < 0. 001.

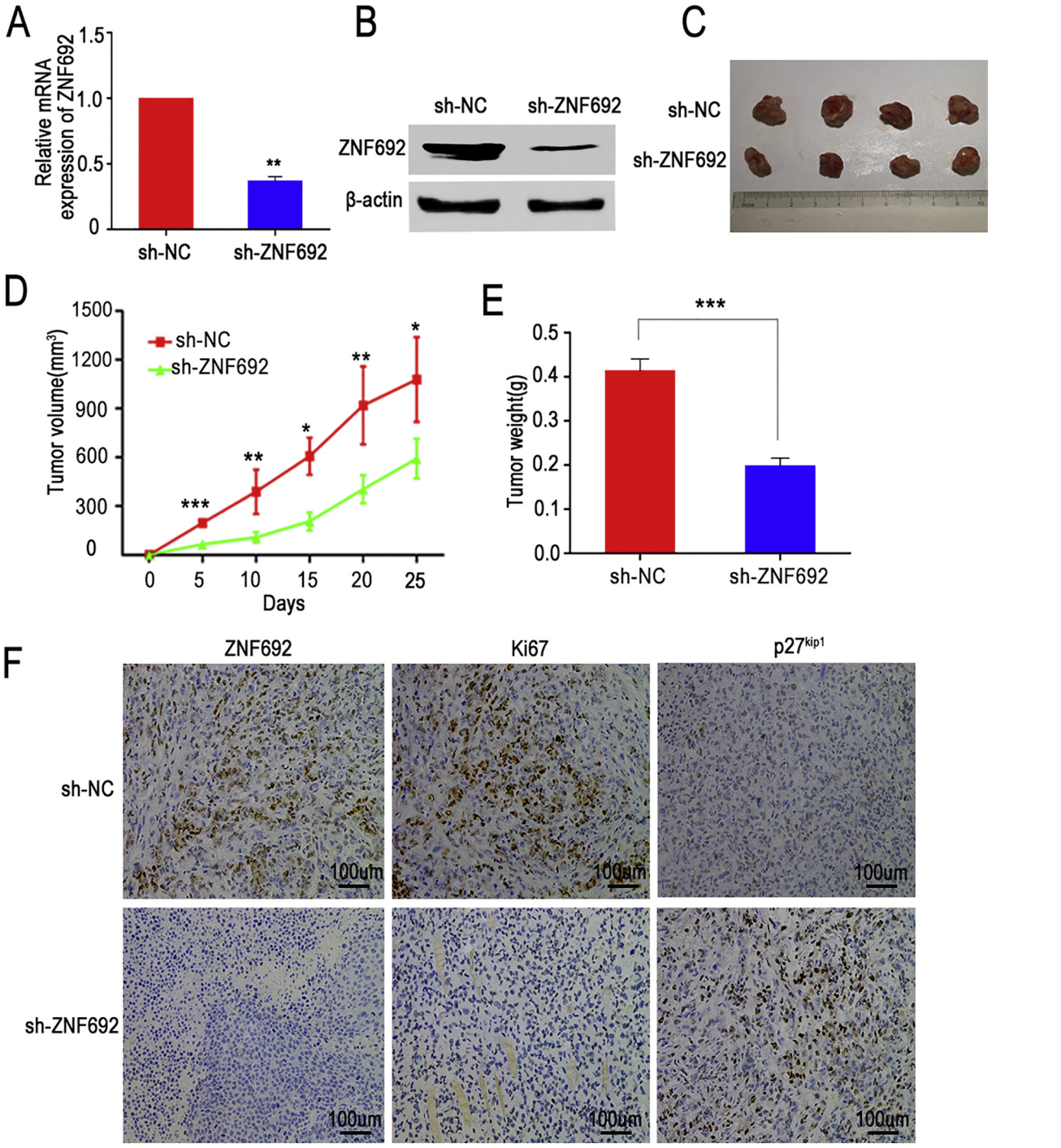

Fig. 6. Knockdown of ZNF692 inhibited tumour growth in vivo. (A–B) The transfection efficiency of sh-ZNF692 was determined by qRT-PCR and Western blotting. (C) A total of eight nude female mice were sacrificed and xenograft tumours were collected 4 weeks after injection. (D-E) Tumour volume and weight were decreased in the sh-ZNF692 group compared with those in the sh-NC group. (F) The expression of ZNF692, Ki-67 was downregulated and $p27^{kip1}$ was upregulated in sh-ZNF692 xenograft tumours as analysed by IHC staining. Error bars represent the mean ± SD values. *P < 0.05, **P < 0.01, ***P < 0.001.

of $p27^{kip1}$ have been widely studied in CC [34,35]. Many studies have also indicated that $p27^{kip1}$ can suppress CDK2-Thr160 phosphorylation [36,37]. Stephanie Mueller et al. [38] found a key mechanism for the adjustment of the G1/S transition via CDK2 phosphorylation at Thr160 in hepatocytes. Our data coincide with preceding studies, showing that si-ZNF692 induces G1 phase arrest by regulating the $p27^{kip1}$ expression. The expression of $p27^{kip1}$, a cell cycle-dependent kinase inhibitor (CDKI), was up-regulated in si-ZNF692 cells, to induce G1 phase arrest accompanied by the down-regulation of P^{Thr160}-CDK2 in si-ZNF692 cells. Meanwhile, decreased $p27^{kip1}$ and increased P^{Thr160}-CDK2 were observed in oe-ZNF692 cells.

The imbalance of p27 expression in cancer has mainly been contributed to proteasomal degradation [39–41]; however, little is known of its disordered expression at the transcription level is little known. Recently, Yawei Li et al. proved that expression of p27 can be transcriptionally upregulated by FOXO1 directly binding to its promoter [42]. Our results showed that si-ZNF692 inhibited proliferation, migration, invasion and G1 phase processes in CC cells mainly by increasing

$p27^{kip1}$ expression. The rescue experiments indicated that knockdown of $p27^{kip1}$ partially recovered the phenotypes in si-ZNF692 HeLa cells. ChIP assay and luciferase reporter assay indicated that ZNF692 directly bound the promoter region of $p27^{kip1}$ at 815-1022 bp to suppress its transcription. Therefore, ZNF692 might have carcinogenic effects partially in a $p27^{kip1}$-dependent manner.

In conclusion, we found that ZNF692 is overexpressed in CC and is positively correlated with advanced TNM stage and lymph node metastasis. It plays an important role in CC progression by promoting the proliferation, invasion and migration of CC cells. With regard to the underlying mechanism, ZNF692 could enhance the cell cycle transition by regulating the $p27^{kip1}$/P^{Thr160}-CDK2 signal pathway. Moreover, ZNF692 directly binds to the promoter region (815-1022 bp) of $p27^{kip1}$ to exert its effect on promoting CC aggressiveness. Our present study adds to the accumulating evidence that ZNF692 exerts a carcinogenic role in CC and could be a potential prognostic biomarker as well as a target for treatment of CC.

Supplementary data to this article can be found online at https://doi.org/10.1016/j.ygyno.2018.11.022.

Author contributions

Lin Xu, Guangfu Jin and Binhui Ren designed the study. Biqing Zhu, Yinpeng Pan and Xiufen Zheng performed the experiment. Quanli Zhang and Yaqin Wu were responsible for graphics. Jing Luo and Qian Li wrote the manuscript. Emei Lu made statistical analysis.

Acknowledgments

This research was supported by the National Natural Science Foundation of China (81672869), Jiangsu Provincial Special Program of Medical Science Funding (BL2012030), Jiangsu Provincial Science Foundation (BK20161596), Jiangsu Provincial Medical Outstanding Talent (Lin Xu) and Jiangsu Provincial Medical Youth Talent (Binhui Ren, QNRC2016657).

References

[1] L.A. Torre, F. Bray, R.L. Siegel, J. Ferlay, J. Lortet-Tieulent, A. Jemal, Global cancer statistics, 2012, CA Cancer J. Clin. 65 (2015) 87–108.
[2] N. Munoz, F.X. Bosch, S. de Sanjose, R. Herrero, X. Castellsague, K.V. Shah, P.J. Snijders, C.J. Meijer, International Agency for Research on Cancer Multicenter Cervical Cancer Study G, Epidemiologic classification of human papillomavirus types associated with cervical cancer, N. Engl. J. Med. 348 (2003) 518–527.
[3] S.M. Wang, Y.L. Qiao, Implementation of cervical cancer screening and prevention in China–challenges and reality, Jpn. J. Clin. Oncol. 45 (2015) 7–11.
[4] O. Ginsburg, R. Badwe, P. Boyle, G. Derricks, A. Dare, T. Evans, A. Eniu, J. Jimenez, T. Kutluk, G. Lopes, S.I. Mohammed, Y.L. Qiao, S.F. Rashid, D. Summers, D. Sarfati, M. Temmerman, E.L. Trimble, A.I. Padela, A. Aggarwal, R. Sullivan, Changing global policy to deliver safe, equitable, and affordable care for women's cancers, Lancet 389 (2017) 871–880.
[5] E.S. Lander, L.M. Linton, B. Birren, C. Nusbaum, M.C. Zody, J. Baldwin, K. Devon, K. Dewar, M. Doyle, W. Fitzhugh, R. Funke, D. Gage, K. Harris, A. Heaford, J. Howland, L. Kann, J. Lehoczky, R. LeVine, P. McEwan, K. McKernan, J. Meldrim, J.P. Mesirov, C. Miranda, W. Morris, J. Naylor, C. Raymond, M. Rosetti, R. Santos, A. Sheridan, C. Sougnez, Y. Stange-Thomann, N. Stojanovic, A. Subramanian, D. Wyman, J. Rogers, J. Sulston, R. Ainscough, S. Beck, D. Bentley, J. Burton, C. Clee, N. Carter, A. Coulson, R. Deadman, P. Deloukas, A. Dunham, I. Dunham, R. Durbin, L. French, D. Grafham, S. Gregory, T. Hubbard, S. Humphray, A. Hunt, M. Jones, C. Lloyd, A. McMurray, L. Matthews, S. Mercer, S. Milne, J.C. Mullikin, A. Mungall, R. Plumb, M. Ross, R. Shownkeen, S. Sims, R.H. Waterston, R.K. Wilson, L.W. Hillier, J.D. McPherson, M.A. Marra, E.R. Mardis, L.A. Fulton, A.T. Chinwalla, K.H. Pepin, W.R. Gish, S.L. Chissoe, M.C. Wendl, K.D. Delehaunty, T.L. Miner, A. Delehaunty, J.B. Kramer, L.L. Cook, R.S. Fulton, D.L. Johnson, P.J. Minx, S.W. Clifton, T. Hawkins, E. Branscomb, P. Predki, P. Richardson, S. Wenning, T. Slezak, N. Doggett, J.F. Cheng, A. Olsen, S. Lucas, C. Elkin, E. Uberbacher, M. Frazier, R.A. Gibbs, D.M. Muzny, S.E. Scherer, J.B. Bouck, E.J. Sodergren, K.C. Worley, C.M. Rives, J.H. Gorrell, M.L. Metzker, S.L. Naylor, R.S. Kucherlapati, D.L. Nelson, G.M. Weinstock, Y. Sakaki, A. Fujiyama, M. Hattori, T. Yada, A. Toyoda, T. Itoh, C. Kawagoe, H. Watanabe, Y. Totoki, T. Taylor, J. Weissenbach, R. Heilig, W. Saurin, F. Artiguenave, P. Brottier, T. Bruls, E. Pelletier, C. Robert, P. Wincker, D.R. Smith, L. Doucette-Stamm, M. Rubenfield, K. Weinstock, H.M. Lee, J. Dubois, A. Rosenthal, M. Platzer, G. Nyakatura, S. Taudien, A. Rump, H. Yang, J. Yu, J. Wang, G. Huang, J. Gu, L. Hood, L. Rowen, A. Madan, S. Qin, R.W. Davis, N.A. Federspiel, A.P. Abola, M.J. Proctor, R.M. Myers, J. Schmutz, M. Dickson, J. Grimwood, D.R. Cox, M.V. Olson, R. Kaul, C. Raymond, N. Shimizu, K. Kawasaki, S. Minoshima, G.A. Evans, M. Athanasiou, R. Schultz, B.A. Roe, F. Chen, H. Pan, J. Ramser, H. Lehrach, R. Reinhardt, W.R. McCombie, M. de la Bastide, N. Dedhia, H. Blocker, K. Hornischer, G. Nordsiek, R. Agarwala, L. Aravind, J.A. Bailey, A. Bateman, S. Batzoglou, E. Birney, P. Bork, D.G. Brown, C.B. Burge, L. Cerutti, H.C. Chen, D. Church, M. Clamp, R.R. Copley, T. Doerks, S.R. Eddy, E.E. Eichler, T.S. Furey, J. Galagan, J.G. Gilbert, C. Harmon, Y. Hayashizaki, D. Haussler, H. Hermjakob, K. Hokamp, W. Jang, L.S. Johnson, T.A. Jones, S. Kasif, A. Kaspryzk, S. Kennedy, W.J. Kent, P. Kitts, E.V. Koonin, I. Korf, D. Kulp, D. Lancet, T.M. Lowe, A. McLysaght, T. Mikkelsen, J.V. Moran, N. Mulder, V.J. Pollara, C.P. Ponting, G. Schuler, J. Schultz, G. Slater, A.F. Smit, E. Stupka, J. Szustakowki, D. Thierry-Mieg, J. Thierry-Mieg, L. Wagner, J. Wallis, R. Wheeler, A. Williams, Y.I. Wolf, K.H. Wolfe, S.P. Yang, R.F. Yeh, F. Collins, M.S. Guyer, J. Peterson, A. Felsenfeld, K.A. Wetterstrand, A. Patrinos, M.J. Morgan, P. de Jong, J.J. Catanese, K. Osoegawa, H. Shizuya, S. Choi, Y.J. Chen, J. Szustakowki, International Human Genome Sequencing C, Initial sequencing and analysis of the human genome, Nature 409 (2001) 860–921.
[6] L. Graff, F. Castrop, M. Bauer, H. Hofler, M. Gratzl, Expression of vesicular monoamine transporters, synaptosomal-associated protein 25 and syntaxin1: a signature of human small cell lung carcinoma, Cancer Res. 61 (2001) 2138–2144.
[7] L. Yang, S.R. Hamilton, A. Sood, T. Kuwai, L. Ellis, A. Sanguino, G. Lopez-Berestein, D.D. Boyd, The previously undescribed ZKSCAN3 (ZNF306) is a novel "driver" of colorectal cancer progression, Cancer Res. 68 (2008) 4321–4330.
[8] F.Y. Lo, J.W. Chang, I.S. Chang, Y.J. Chen, H.S. Hsu, S.F. Huang, F.Y. Tsai, S.S. Jiang, R. Kanteti, S. Nandi, R. Salgia, Y.C. Wang, The database of chromosome imbalance regions and genes resided in lung cancer from Asian and Caucasian identified by array-comparative genomic hybridization, BMC Cancer 12 (2012) 235.
[9] Y. Li, Q. Zhao, L.Q. Fan, L.L. Wang, B.B. Tan, Y.L. Leng, Y. Liu, D. Wang, Zinc finger protein 139 expression in gastric cancer and its clinical significance, World J. Gastroenterol. 20 (2014) 18346–18353.
[10] E. Inoue, J. Yamauchi, AMP-activated protein kinase regulates PEPCK gene expression by direct phosphorylation of a novel zinc finger transcription factor, Biochem. Biophys. Res. Commun. 351 (2006) 793–799.
[11] C.C. Huang, S. Gadd, N. Breslow, C. Cutcliffe, S.T. Sredni, I.B. Helenowski, J.S. Dome, P.E. Grundy, D.M. Green, M.K. Fritsch, E.J. Perlman, Predicting relapse in favorable histology Wilms tumor using gene expression analysis: a report from the Renal Tumor Committee of the Children's Oncology Group, Clin. Cancer Res. 15 (2009) 1770–1778.
[12] M.P. Tremblay, V.E. Armero, A. Allaire, S. Boudreault, C. Martenon-Brodeur, M. Durand, E. Lapointe, P. Thibault, M. Tremblay-Letourneau, J.P. Perreault, M.S. Scott, M. Bisaillon, Global profiling of alternative RNA splicing events provides insights into molecular differences between various types of hepatocellular carcinoma, BMC Genomics 17 (2016) 683.
[13] Q. Zhang, X. Zheng, Q. Sun, R. Shi, J. Wang, B. Zhu, L. Xu, G. Zhang, B. Ren, ZNF692 promotes proliferation and cell mobility in lung adenocarcinoma, Biochem. Biophys. Res. Commun. 490 (2017) 1189–1196.
[14] M. Goldman, B. Craft, T. Swatloski, M. Cline, O. Morozova, M. Diekhans, D. Haussler, J. Zhu, The UCSC Cancer Genomics Browser: update 2015, Nucleic Acids Res. 43 (2015) D812–D817.
[15] D.W. Huang, B.T. Sherman, Q. Tan, J. Kir, D. Liu, D. Bryant, Y. Guo, R. Stephens, M.W. Baseler, H.C. Lane, R.A. Lempicki, DAVID bioinformatics resources: expanded annotation database and novel algorithms to better extract biology from large gene lists, Nucleic Acids Res. 35 (2007) W169–W175.
[16] B.T. Sherman, W. Huang Da, Q. Tan, Y. Guo, S. Bour, D. Liu, R. Stephens, M.W. Baseler, H.C. Lane, R.A. Lempicki, DAVID knowledgebase: a gene-centered database integrating heterogeneous gene annotation resources to facilitate high-throughput gene functional analysis, BMC Bioinf. 8 (2007) 426.
[17] C. Yuan, Y. Bu, C. Wang, F. Yi, Z. Yang, X. Huang, L. Cheng, G. Liu, Y. Wang, F. Song, NFBD1/MDC1 is a protein of oncogenic potential in human cervical cancer, Mol. Cell. Biochem. 359 (2012) 333–346.
[18] X. Yang, Z. Zhang, M. Qiu, J. Hu, X. Fan, J. Wang, L. Xu, R. Yin, Glypican-5 is a novel metastasis suppressor gene in non-small cell lung cancer, Cancer Lett. 341 (2013) 265–273.
[19] D. Kho, C. MacDonald, R. Johnson, C.P. Unsworth, S.J. O'Carroll, E. du Mez, C.E. Angel, E.S. Graham, Application of xCELLigence RTCA biosensor technology for revealing the profile and window of drug responsiveness in real time, Biosensors (Basel) 5 (2015) 199–222.
[20] F. Chehrehasa, A.C. Meedeniya, P. Dwyer, G. Abrahamsen, A. Mackay-Sim, EdU, a new thymidine analogue for labelling proliferating cells in the nervous system, J. Neurosci. Methods 177 (2009) 122–130.
[21] K.H. Kim, J.M. Sederstrom, Assaying cell cycle status using flow cytometry, Curr Protoc Mol Biol 111 (2015) 28 26 21–11.
[22] R. Tupler, G. Perini, M.R. Green, Expressing the human genome, Nature 409 (2001) 832–833.
[23] J. Russo, J. Santucci-Pereira, I.H. Russo, The genomic signature of breast cancer prevention, Genes (Basel) 5 (2014) 65–83.
[24] D. Hanahan, R.A. Weinberg, The hallmarks of cancer, Cell 100 (2000) 57–70.
[25] A.L. Krasnoselsky, C.C. Whiteford, J.S. Wei, S. Bilke, F. Westermann, Q.R. Chen, J. Khan, Altered expression of cell cycle genes distinguishes aggressive neuroblastoma, Oncogene 24 (2005) 1533–1541.
[26] M. Li, F. Zhang, X. Wang, X. Wu, B. Zhang, N. Zhang, W. Wu, Z. Wang, H. Weng, S. Liu, G. Gao, J. Mu, Y. Shu, R. Bao, Y. Cao, J. Lu, J. Gu, J. Zhu, Y. Liu, Magnolol inhibits growth of gallbladder cancer cells through the p53 pathway, Cancer Sci. 106 (2015) 1341–1350.
[27] M.G. Vander Heiden, L.C. Cantley, C.B. Thompson, Understanding the Warburg effect: the metabolic requirements of cell proliferation, Science 324 (2009) 1029–1033.

[28] M. Jain, R. Nilsson, S. Sharma, N. Madhusudhan, T. Kitami, A.L. Souza, R. Kafri, M.W. Kirschner, C.B. Clish, V.K. Mootha, Metabolite profiling identifies a key role for glycine in rapid cancer cell proliferation, Science 336 (2012) 1040–1044.
[29] L. Cai, B.P. Tu, Driving the cell cycle through metabolism, Annu. Rev. Cell Dev. Biol. 28 (2012) 59–87.
[30] C. Sun, G. Wang, K.H. Wrighton, H. Lin, Z. Songyang, X.H. Feng, X. Lin, Regulation of p27Kip1 phosphorylation and G1 cell cycle progression by protein phosphatase PPM1G, Am. J. Cancer Res. 6 (2016) 2207–2220.
[31] C.J. Sherr, The Pezcoller lecture: cancer cell cycles revisited, Cancer Res. 60 (2000) 3689–3695.
[32] H. Nguyen, D.M. Gitig, A. Koff, Cell-free degradation of p27(kip1), a G1 cyclin-dependent kinase inhibitor, is dependent on CDK2 activity and the proteasome, Mol. Cell. Biol. 19 (1999) 1190–1201.
[33] L.C. Ooi, N. Watanabe, Y. Futamura, S.F. Sulaiman, I. Darah, H. Osada, Identification of small molecule inhibitors of p27(Kip1) ubiquitination by high-throughput screening, Cancer Sci. 104 (2013) 1461–1467.
[34] R. Stanculescu, M. Ceausu, Z. Ceausu, V. Bausic, Immunofluorescence expression of Ki-67, p53 and cyclin inhibitors (p16ink4a, p21 and p27) in low-grade cervical lesions versus high-grade cervical lesions. Research study on cell cultures, Romanian J. Morphol. Embryol. 54 (2013) 725–734.
[35] J. Bouda, O. Hes, M. Koprivova, M. Pesek, T. Svoboda, L. Boudova, P27 as a prognostic factor of early cervical carcinoma, Int. J. Gynecol. Cancer 23 (2013) 164–169.
[36] T. Abbas, S. Jha, N.E. Sherman, A. Dutta, Autocatalytic phosphorylation of CDK2 at the activating Thr160, Cell Cycle 6 (2007) 843–852.
[37] D.O. Morgan, Principles of CDK regulation, Nature 374 (1995) 131–134.
[38] S. Mueller, J. Huard, K. Waldow, X. Huang, L.A. D'Alessandro, S. Bohl, K. Borner, D. Grimm, S. Klamt, U. Klingmuller, M. Schilling, T160-phosphorylated CDK2 defines threshold for HGF dependent proliferation in primary hepatocytes, Mol. Syst. Biol. 11 (2015) 795.
[39] I.M. Chu, L. Hengst, J.M. Slingerland, The Cdk inhibitor p27 in human cancer: prognostic potential and relevance to anticancer therapy, Nat. Rev. Cancer 8 (2008) 253–267.
[40] C.M. Das, P. Taylor, M. Gireud, A. Singh, D. Lee, G. Fuller, L. Ji, J. Fangusaro, V. Rajaram, S. Goldman, C. Eberhart, V. Gopalakrishnan, The deubiquitylase USP37 links REST to the control of p27 stability and cell proliferation, Oncogene 32 (2013) 1691–1701.
[41] Y. Li, J. Huang, B. Zeng, D. Yang, J. Sun, X. Yin, M. Lu, Z. Qiu, W. Peng, T. Xiang, H. Li, G. Ren, PSMD2 regulates breast cancer cell proliferation and cell cycle progression by modulating p21 and p27 proteasomal degradation, Cancer Lett. 430 (2018) 109–122.
[42] G. Jiang, C. Huang, J. Li, H. Huang, J. Wang, Y. Li, F. Xie, H. Jin, J. Zhu, C. Huang, Transcriptional and post-transcriptional upregulation of p27 mediates growth inhibition of isorhapontigenin (ISO) on human bladder cancer cells, Carcinogenesis 39 (2018) 482–492.